Atmos. Chem. Phys., 22, 14799–14811, 2022
https://doi.org/10.5194/acp-22-14799-2022

Atmospheric Chemistry and Physics
Open Access
EGU

Examining the implications of photochemical indicators for O_3–NO_x–VOC sensitivity and control strategies: a case study in the Yangtze River Delta (YRD), China

Xun Li[1], Momei Qin[1], Lin Li[1], Kangjia Gong[1], Huizhong Shen[2], Jingyi Li[1], and Jianlin Hu[1]

[1]Jiangsu Key Laboratory of Atmospheric Environment Monitoring and Pollution Control, Collaborative Innovation Center of Atmospheric Environment and Equipment Technology, Nanjing University of Information Science and Technology, Nanjing, 210044, China
[2]School of Environmental Sciences and Engineering, Southern University of Science and Technology, Shenzhen, 518055, China

Correspondence: Momei Qin (momei.qin@nuist.edu.cn) and Jianlin Hu (jianlinhu@nuist.edu.cn)

Received: 11 July 2022 – Discussion started: 22 July 2022
Revised: 19 September 2022 – Accepted: 20 October 2022 – Published: 22 November 2022

Abstract. Ozone (O_3) has become a significant air pollutant in China in recent years. O_3 abatement is challenging due to the nonlinear response of O_3 to precursors nitrogen oxides (NO_x) and volatile organic compounds (VOCs). Photochemical indicators are widely used to estimate the O_3–NO_x–VOC sensitivity, and this has important policy implications. However, the effectiveness of the indicators has seldom been evaluated. This study examined the applications of four indicators that include the ratio of the production rates of H_2O_2 and HNO_3 ($P_{H_2O_2}/P_{HNO_3}$), HCHO/NO_2, HCHO/NO_y, and reactive nitrogen (NO_y) in the Yangtze River Delta (YRD) with localized thresholds. The overall accuracy was high (> 92 %) for all indicators and not significantly reduced with different simulation periods or in different locations of the region. By comparing with the O_3 isopleths, it was found that HCHO/NO_2 and HCHO/NO_y showed the most consistency, whereas $P_{H_2O_2}/P_{HNO_3}$ (NO_y) tended to underestimate (overestimate) the positive response of O_3 to NO_x. Additionally, $P_{H_2O_2}/P_{HNO_3}$ was less likely to attribute the O_3 formation to mixed sensitivity than the other indicators, and this demonstrated a preference for a single-pollutant control strategy. This study also revealed that the details in the methodology used to derive the threshold values impacted the results, and this may produce uncertainties in the application of photochemical indicators.

1 Introduction

Ozone (O_3) is one of the most important pollutants in the atmosphere, high concentrations of which pose a serious threat to human health, ecosystems, and global climate change (Y. Wang et al., 2020; Liang et al., 2019; De Marco et al., 2022; Feng et al., 2022; Skeie et al., 2020). Many metropolitan areas in China, such as Beijing–Tianjin–Hebei (BTH), the Yangtze River Delta (YRD), and the Pearl River Delta (PRD), have been experiencing severe O_3 pollution in recent years (Gao et al., 2017; Lu et al., 2018). Moreover, unlike the decline in fine particulate matter ($PM_{2.5}$), the O_3 concentrations in urban areas have increased (Wang et al., 2019; Lu et al., 2020; Li et al., 2020).

O_3 is produced by photochemical reactions involving nitrogen oxides (NO_x) and volatile organic compounds (VOCs). However, the response of O_3 to either precursor is nonlinear due to the changing roles of NO_x and VOCs with different VOC/NO_x ratios in O_3 chemistry, making O_3 pollution abatement more challenging (Wang et al., 2011; Liu et al., 2013). Briefly, when O_3 increases with a reduction (increase) in NO_x (VOCs), O_3 formation is in a NO_x-saturated or VOC-limited regime that tends to occur in urban areas or cold seasons with relatively low VOC/NO_x ratios (Tan et al., 2018; Sillman, 1995). Conversely, O_3 decreases with

reduced NO_x and is typically insensitive to VOC levels in a NO_x-limited regime. This is often the case in rural and remote regions with lower NO_x emissions (Murphy et al., 2007; Sillman, 1999). Importantly, a reduction in either NO_x or VOCs can lead to less O_3 production when the O_3 formation regime is shifted from one to the other, and this is referred to as the transitional regime (Chen et al., 2021; Jin and Holloway, 2015).

Many approaches, including photochemical indicators, the observation-based modeling method (OBM), and the emission-based method (EBM), have been developed to predict O_3–NO_x–VOC sensitivity (Sillman, 2002; M. Wang et al., 2020; Shen et al., 2021). Among these approaches, the values of the photochemical indicators (such as VOC/NO_x, the ratios of hydrogen peroxide to nitric acid (H_2O_2/HNO_3) or production rates of H_2O_2 and HNO_3 ($P_{H_2O_2}/P_{HNO_3}$), the ratios of formaldehyde to nitrogen dioxide or reactive nitrogen ($HCHO/NO_2$ or $HCHO/NO_y$), the O_3-to-nitric-acid ratios (O_3/HNO_3), and NO_y) can be derived directly from ground-based measurements, chemical transport models, or even satellite measurements if available and thus have been widely used in previous studies (Martin et al., 2004; Jin and Holloway, 2015; Jiménez and Baldasano, 2004; Sillman, 2002; Liu et al., 2010b). For instance, Ye et al. (2021) presented hourly H_2O_2/NO_z ($NO_z = NO_y - NO_x$) ratios based on measurements at Mount Tai and found that O_3 formation was VOC-limited in the morning ($H_2O_2 / NO_z < 0.15$) and switched to NO_x-limited ($H_2O_2 / NO_z > 0.2$) in the afternoon. The ratio H_2O_2/HNO_3 is considered one of the most robust indicators to determine O_3 sensitivity, while the thresholds are highly variable for different regions (Peng et al., 2011; Xie et al., 2014; Ye et al., 2016). $P_{H_2O_2}/P_{HNO_3}$ is primarily used in modeling work, such as the spatial distribution of O_3 formation regimes over the modeling domain that was exhibited with the indicator (Liu et al., 2010a; Du et al., 2022; Zhang et al., 2020). Based on long-term measurements of HCHO and NO_2 columns from satellites, Jin and Holloway (2015) found that near-surface O_3 formation in several megacities in China had changed from VOC-limited in 2005 to transitional in 2013 with reduced NO_2.

The thresholds of photochemical indicators that split VOC-limited, transitional, and NO_x-limited regimes vary from region to region, largely depending on local emissions and possibly related to meteorological conditions as well. It was found that the primary emissions of HCHO increased the value of $HCHO/NO_2$, and therefore the O_3 sensitivity determined by the ratio could have been biased with given thresholds. For example, some VOC-limited regimes are misclassified as transitional (Liu et al., 2021). Du et al. (2022) compared the spatial distribution of O_3 sensitivity regimes diagnosed using different indicators and pointed out that $P_{H_2O_2}/P_{HNO_3}$ could be more affected by local emissions than $HCHO/NO_2$. As H_2O_2 and HNO_3 are very soluble and susceptible to deposition and aerosol formation, the indicator values that involve the two species may change with the meteorological conditions (Castell et al., 2009). However, certain thresholds were often used without considering the variability, such as the range of one to two for $HCHO/NO_2$ (Jin and Holloway, 2015; Tang et al., 2012; Ma et al., 2021). In particular, the integrated source apportionment method (ISAM) implemented in the Community Multiscale Air Quality (CMAQ) model attributes O_3 production to either VOC or NO_x tracers based on a comparison of the instantaneous $P_{H_2O_2}/P_{HNO_3}$ with 0.35, and this ultimately affects the source apportionment of O_3 using ISAM (Kwok et al., 2015). Whether photochemical indicators can accurately predict O_3 sensitivity to precursors with given threshold values has seldom been examined.

In light of the above, this work aimed to revisit the effectiveness of photochemical indicators in the prediction of the O_3-precursor response based on a case study in the YRD region in eastern China. Specifically, the work deployed the most used method to derive localized thresholds of the four photochemical indicators (i.e., $P_{H_2O_2}/P_{HNO_3}$, $HCHO/NO_2$, $HCHO/NO_y$, and NO_y) for Jiangsu Province in the YRD, which has been experiencing severe photochemical pollution (Qin et al., 2021; Xu et al., 2021; Lu et al., 2018). The assessment was conducted to examine three aspects: (1) whether the localized threshold values are appropriate for a different location or a different year, (2) the consistency of the photochemical indicator approach with O_3 isopleths plots for predicting the O_3–NO_x–VOC response, and (3) possible uncertainties induced by the methodology with which the threshold values are determined. This work can provide insight into the use of photochemical indicators in understanding O_3 formation and making effective strategies for emission control.

2 Methods

2.1 Model configurations

The CMAQ model version 5.2 was applied to simulate the photochemical pollution over the YRD and its surrounding areas (Fig. 1) in July 2017. The simulation was performed at a 4 km resolution, using the chemical mechanism of saprc07tic. A regional O_3 pollution event that occurred from 22 to 31 July with the mean level of the observed daily maximum 8 h average (MDA8) O_3 exceeding 85 ppb over the YRD was selected to study the relationship between the O_3–NO_x–VOC sensitivity and the values of the photochemical indicators. The CMAQ model was driven by a mesoscale meteorological model, the Weather Research and Forecasting (WRF) version 4.2.2. The 2017 emission inventory of anthropogenic air pollutants in the YRD compiled by the Shanghai Academy of Environmental Sciences (An et al., 2021) was adopted, with the details of the other emissions (i.e., biogenic emissions and open burning) found in Hu et al. (2016).

Figure 1. The simulation domain. The blue area indicates the YRD including Jiangsu, Anhui, Shanghai, and Zhejiang. Three representative sites of Caochangmen (CCM), Zhonghuamen (ZHM), and Laoshan (LS) are marked.

2.2 Model performance evaluation

The model performance on O_3 was examined by comparing the simulation with observational data at the monitoring sites supervised by the China National Environmental Monitoring Center (CNEMC) in 13 cities in Jiangsu Province. Three metrics (the normalized mean bias (NMB), the normalized mean error (NME), and the correlation coefficient (r)) as in Sheng et al. (2022) were calculated to evaluate the agreement between the simulation and observations. The criteria of the model performance were recommended by Emery et al. (2017). Table S1 in the Supplement shows that the NMB (NME) values in 12 (10) out of 13 cities met the criteria, indicating that the overall performance was good. In general, the model overestimated O_3, with the NMB in the range of $-2\,\%$ to $17\,\%$. The correlations of the simulation with the observations (all r values above 0.5) indicated that hourly variations in the simulation agree well with the observations. Additionally, three sites in Nanjing (a megacity in Jiangsu), including Caochangmen (CCM), Zhonghuamen (ZHM), and Laoshan (LS), representing downtown, upwind, and downwind areas of the city (see Fig. 1), respectively, were selected to examine the consistency between the photochemical indicators and the O_3 isopleths in the implication of O_3-precursor sensitivities. Figure S1 in the Supplement shows that the model well reproduced the O_3 pollution events at the three sites during the simulation period.

Other species involved in the photochemical indicators, such as HCHO, HNO_3, NO_2, and NO_y (NO_y (g)=NO+NO_2+NO_3+2×N_2O_5+HONO+HNO_3+HNO_4+peroxyacetyl nitrate and its homologs (PANs)+alkyl nitrates (ANs) and nitrogen oxychlorides ($ClNO_x$) in the model), were examined and compared with observations during the EXPLORE-YRD campaign (Li et al., 2021; Sun et al., 2022). Figure S2 shows that HCHO was underestimated by $51\,\%$, while NO_2 and NO_y were slightly overestimated, with NMBs of $16\,\%$ and $7\,\%$, respectively. The anthropogenic emission inventory and model were set up as in the simulation for the EXPLORE-YRD campaign, and the simulated ratios of HCHO/NO_2 and HCHO/NO_y in this study could have been underestimated. In addition, the simulation could represent an environment with less abundant VOCs than in the real atmosphere over the YRD.

2.3 Determination of the indicator thresholds

The use of photochemical indicators requires threshold values that differentiate O_3 formation regimes. In this study, the thresholds of the indicators were derived based on the association of the O_3 reduction relative to the baseline emission scenario resulting from NO_x or VOC emission reductions (i.e., $\Delta O_{3\,NO_x}$ or $\Delta O_{3\,VOC}$), with concurrent indicator values at all grid cells in Jiangsu Province. Therefore, two additional runs with either a $35\,\%$ decrease in NO_x or a $35\,\%$ decrease in VOC emissions were performed following Sillman et al. (1998) and other studies (Xie et al., 2014; Peng et al., 2011). The resulting O_3 changes ($\Delta O_{3\,NO_x}$ and $\Delta O_{3\,VOC}$) were obtained to identify the O_3 formation regimes at each grid cell, with the criteria given in Table 1. It should be noted that the average changes in O_3 during 13:00–16:00 LT (local time) during the simulation period were used when O_3 peaked and was of most concern.

This study focused on four photochemical indicators that are frequently used, including $P_{H_2O_2}/P_{HNO_3}$, HCHO/NO_2, HCHO/NO_y, and NO_y, with the underlying mechanisms extensively described in the literature (Xie et al., 2014; Kwok et al., 2015; Sillman, 1995; Duncan et al., 2010). The indicator values for each grid cell were calculated based on the simulated concentrations of related species, except for $P_{H_2O_2}/P_{HNO_3}$, which were obtained using the integrated reaction rate (IRR) of the CMAQ process analysis tool (Gipson and Young, 1999). The percentile distribution of the indicator values for the VOC-limited grid cells and the NO_x-limited grid cells were examined individually. The photochemical indicators typically showed higher values at NO_x-limited grid cells than in VOC-limited locations. Finally, the thresholds of a certain indicator were determined using the 95th-percentile value of the indicator for the VOC-limited grid cells and the 5th-percentile value for the NO_x-limited grid cells as the lower and upper limits of the transition intervals, respectively. Indicator values lower than the transition intervals suggested O_3 formation was VOC-limited, while higher values than the transition intervals were associated with NO_x-limited regimes. In some cases, the 95th-percentile VOC-limited value was higher than the 5th-percentile NO_x-

Table 1. Identification of the O_3 formation regimes at each grid cell based on the O_3 changes resulting from perturbed emissions as in Sillman et al. (1998) or the sensitivity coefficients using the high-order decoupled direct method (HDDM) as in Wang et al. (2011).

Method	O_3 formation regime	Definition
Perturbed simulations	VOC-limited	$\Delta O_{3\,VOC} \geq 5$ ppb and $(\Delta O_{3\,VOC} - \Delta O_{3\,NO_x}) \geq 5$ ppb
	NO_x-limited	$\Delta O_{3\,NO_x} \geq 5$ ppb and $(\Delta O_{3\,NO_x} - \Delta O_{3\,VOC}) \geq 5$ ppb
High-order decoupled direct method (HDDM)	VOC-limited	$S1_{VOCs} \geq 5$ ppb and $(S1_{VOCs} - S1_{NO_x}) \geq 5$ ppb
	NO_x-limited	$S1_{NO_x} \geq 5$ ppb and $(S1_{NO_x} - S1_{VOCs}) \geq 5$ ppb

limited value, indicating the indicator was invalid and could not be used to determine the O_3 sensitivity properly.

2.4 Evaluation of the indicators

2.4.1 Evaluation metrics

The feasibility of a given threshold for an indicator applied throughout a region or over a short-term period (the order of 1–2 years) was evaluated in this study. Some metrics have been developed to estimate the uncertainties in the determination of O_3 regimes using photochemical indicators (Wang et al., 2011; Ye et al., 2016). This work applied Error A, Error B, and the overall accuracy (OA) in Ye et al. (2016) for the evaluation, with the equations given in Table 2. For example, ErrA_NO_x describes the situation where among all grid cells (colored areas in Fig. 2d) with indicator values higher than the upper limit of the transition interval (i.e., assigned to NO_x-limited regimes with the indicator), there existed VOC-limited grid cells that were incorrectly assigned to the NO_x-limited regime. ErrB_NO_x estimates the fraction of the NO_x-limited grid cells (blue areas in Fig. 2d) that were not classified as a NO_x-limited regime since the corresponding indicator values were lower than the upper threshold. ErrA_VOC and ErrB_VOC were defined analogously. OA describes the fraction of all correctly classified grid cells using the indicator at all VOC- or NO_x-limited grid cells.

The indicator evaluation was conducted for the simulation in 2017 (see Sect. 2.1). Additionally, a simulation for the same period (over 22–31 July) in 2018, which has an identical model configuration and identical inputs in all aspects except for the meteorology, was performed for the evaluation as well. Thus, applications of the photochemical indicators with derived thresholds in a different location within the region, in a different year, or with changes in both can be examined separately. This provided insight into the uncertainties associated with emissions or meteorology.

2.4.2 O_3 isopleths

The O_3–NO_x–VOC sensitivity determined by photochemical indicators was compared with the O_3 isopleths that describe the nonlinear relationship between O_3 and the precursors and inform decision makers of emission control strategies in a different manner. The response of O_3 to the domain-wide reductions in VOC and NO_x emissions at three representative sites (CCM, ZHM, and LS) during 13:00–16:00 LT during the simulation period was investigated. Specifically, a total of 36 emission scenarios with anthropogenic VOC and NO_x emissions reduced by 0 %, 20 %, 40 %, 60 %, 80 %, and 100 %, both singly and in combination, were simulated to construct the O_3 isopleth diagram. The O_3 formation regimes based on the thresholds derived in Sect. 2.3 were indicated with color and overlapped with the isopleths.

2.5 Uncertainties in the thresholds

In Sect. 2.3, the O_3 formation regimes were presumably identified according to changes in O_3 with the emission reductions, while the rules could be different in detail. For example, Liang et al. (2006) examined changes in the 8 h O_3 with a 25 % reduction in VOC or NO_x emissions instead of the 1 h O_3 with 35 % reductions as in Sillman (1995). Accordingly, the criteria changed from 5 to 2.5 ppb. Zhang et al. (2020) explored the correlation of indicator values with the relative O_3 changes resulting from a 50 % reduction in the NO_x or VOC emissions. Du et al. (2022) applied the decoupled direct method (DDM) to investigate the sensitivity of O_3 to precursors, instead of perturbing emissions. The impacts on the derived thresholds of the indicators were explored by conducting a few individual tests:

1. The criteria for the O_3 reduction (see Table 1) were set at 2, 3, and 6 ppb.

2. The relative changes in O_3 were examined using the criteria of 2 %, 5 %, and 8 % instead of an absolute change of 5 ppb.

3. The 35 % emission reduction scenarios were replaced with a 20 % and a 40 % reduction in the VOC or NO_x emissions.

4. The high-order decoupled direct method (HDDM) was adopted to split the O_3 formation regimes in two manners referred to as "DDM1" and "DDM2". The HDDM can quantify the responsiveness of air pollutants to infinitesimal perturbations of a model parameter or input (e.g., an emission rate of a precursor) with sensitivity coefficients (Cohan et al., 2005). In this study, the

Table 2. Metrics of the indicator performance evaluation provided in Ye et al. (2016).

Metric	Equation
Error A_NO_x	$\frac{\text{number of VOC-limited grid cells with indicator values above the upper threshold}}{\text{number of all } NO_x\text{-limited and VOC-limited grid cells with indicator values above the upper threshold}} \times 100\,\%$
Error B_NO_x	$\frac{\text{number of } NO_x\text{-limited grid cells with indicator values below the upper threshold}}{\text{number of all } NO_x\text{-limited grid cells}} \times 100\,\%$
Error A_VOC	$\frac{\text{number of } NO_x\text{-limited grid cells with indicator values below the lower threshold}}{\text{number of all } NO_x\text{-limited and VOC-limited grid cells with indicator values below the lower threshold}} \times 100\,\%$
Error B_VOC	$\frac{\text{number of VOC-limited grid cells with indicator values above the lower threshold}}{\text{number of all VOC-limited grid cells}} \times 100\,\%$
OA	$\text{OA} = \frac{\text{number of VOC-limited grid cells with indicator values below the lower threshold + Number of } NO_x\text{-limited grid cells with indicator values above the upper threshold}}{\text{number of all } NO_x\text{-limited and VOC-limited grid cells}} \times 100\,\%$

HDDM estimated the first- and second-order sensitivity coefficients of O_3 to NO_x and VOCs (i.e., $S1_{NO_x}$, $S1_{VOCs}$, $S2_{NO_x}$, $S2_{VOCs}$). With the DDM1 approach, the NO_x-limited locations were defined as those grid cells where S1 NO_x was higher than 5 ppb and at least 5 ppb higher than S1 VOCs (Table 1), following Wang et al. (2011). The VOC-limited grid cells were defined similarly. The DDM2 approach estimated O_3 changes with 35 % reductions in emissions via the Taylor series expansions (Cohan et al., 2005) instead of the perturbed simulations.

3 Results and discussion

3.1 Threshold values of the photochemical indicators

The changes in the O_3 concentrations when reducing VOC or NO_x emissions were used to determine the O_3 formation regimes. Figure 2a shows that high O_3 concentrations (averaged from 13:00 to 16:00 LT during 22–31 July) primarily occurred along the Yangtze River and southern Jiangsu, and O_3 in northern Jiangsu was relatively low. The NO_x emission reduction predominantly led to O_3 decreases in Jiangsu, while only a few locations, such as near the estuary of the Yangtze River, showed an increased O_3 relative to the base case (Fig. 2b). The VOC emission reductions resulted in less significant O_3 decreases compared to the NO_x reduction scenario (Fig. 2c). The O_3 sensitivity regime for each grid cell in Jiangsu was identified with the method described in Sect. 2.3 (Fig. 2d). The O_3 formation in central and southern Jiangsu, where O_3 is abundant, is typically NO_x-limited as a result of a relatively low NO_x concentration in the afternoon (Duncan et al., 2010; Jin et al., 2017; Jin and Holloway, 2015). Some areas along (and on) the Yangtze River were characterized to be VOC-limited regimes, with substantial emissions of NO_x from ship emissions and industry (Sheng et al., 2022). However, not all grid cells in Jiangsu were assigned to the VOC- or NO_x-limited regimes. The white areas in Jiangsu in Fig. 2d indicate that O_3 was insensitive to both NO_x and VOCs (i.e., $\Delta O_{3\,VOC} < 5$ and $\Delta O_{3\,NO_x} < 5$ ppb);

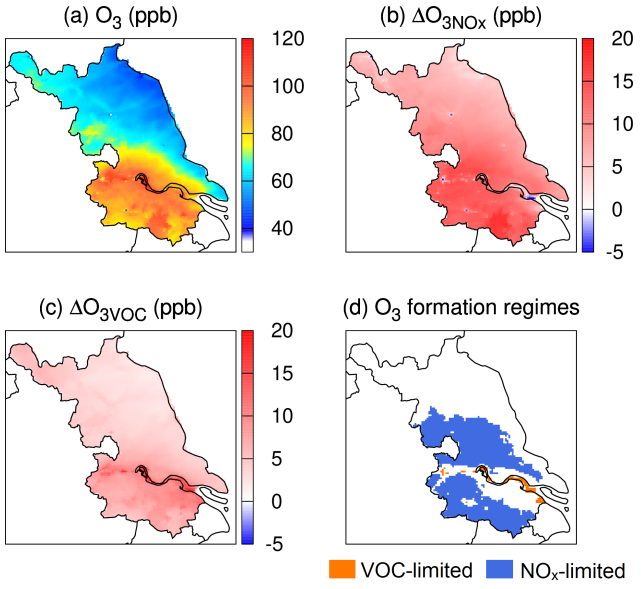

Figure 2. **(a)** Simulated spatial distribution of O_3 averaged from 13:00 to 16:00 LT. during 22–31 July in Jiangsu Province; **(b–c)** O_3 reduction due to a 35 % reduction in domain-wide NO_x and VOC emissions, respectively; **(d)** O_3 formation regimes determined with perturbed simulations.

alternatively, O_3 was sensitive to NO_x (VOC) emissions but showed small changes in O_3 with the perturbation of NO_x (VOC) relative to the VOC (NO_x) reduction scenario (i.e., $|\Delta O_{3\,VOC} - \Delta O_{3\,NO_x}| < 5$ ppb).

The O_3 reductions ($\Delta O_{3\,NO_x}$ or $\Delta O_{3\,VOC}$) against photochemical indicator values at all grid cells over the domain were examined (Fig. 3). The mean values of the $\Delta O_{3\,NO_x}$ slightly increased with higher $P_{H_2O_2}/P_{HNO_3}$, while the $\Delta O_{3\,VOC}$ values showed a decreasing trend, indicating that a reduction in NO_x (VOC) emissions became more (less) effective for O_3 abatement in the locations with higher indicator values. Other indicators displayed a similar pattern except for NO_y, which displayed an opposite result. Due to the contrasting dependence of the $\Delta O_{3\,NO_x}$ and the $\Delta O_{3\,VOC}$ on the indicator values, the thresholds of the photochemical

indicators that separate the O_3 formation regimes were determined (Table 3 and vertical lines in Fig. 3). The localized thresholds for $P_{H_2O_2}/P_{HNO_3}$ [0.55, 0.75] were remarkably higher than that implemented in the model, i.e., 0.35, which would lead to misattribution of the VOC-limited or the transitional regime to the NO_x-limited regime in some locations if the single value was directly used. The thresholds differed from those proposed by researchers in other countries, and some regions in China had significantly distinct thresholds as well (Du et al., 2022; Zhang et al., 2020; Tonnesen and Dennis, 2000a; Liu et al., 2010a).

This work revisited other photochemical indicators including the surface $HCHO/NO_2$, $HCHO/NO_y$, and NO_y. The transition interval of $HCHO/NO_2$ was determined as [0.81, 1.35], showing a higher and wider range than in other work (Jin et al., 2017; Liu et al., 2021; Du et al., 2022) but relative consistency with Tonnesen and Dennis (2000b). It is worth noting that the values mentioned above are all based on measurements or simulations at the ground level, while column $HCHO/NO_2$ retrieved from satellite measurements are more widely used, with thresholds of [1, 2] (Jin and Holloway, 2015; Jin et al., 2017; Duncan et al., 2010; Wang et al., 2021). The transition range for the column $HCHO/NO_2$ is typically broader than that for the surface ratio, e.g., the former of [1.17, 2.42] versus the latter of [0.36, 0.45] in East China (Du et al., 2022). The thresholds of $HCHO/NO_y$ and NO_y in this study were [0.38, 0.60] and [8.18, 17.63], respectively, comparable to the values proposed previously. The comparison shown in Table 3 suggests that the thresholds were mostly location-specific, possibly as they are dependent on atmospheric conditions and emission features. However, the methodology that is used to derive thresholds can also lead to distinct threshold values, and this is discussed in Sect. 3.4.

The spatial distributions of the O_3 formation regimes identified by the photochemical indicators with localized thresholds are exhibited in Fig. 4. Most of the areas in Jiangsu ($> 80\,\%$ of the grid cells covering Jiangsu, Table S2) were attributed to NO_x-limited regimes in terms of the summertime O_3 formation in the afternoon using all indicators. A few urban centers and some locations near the Yangtze River were identified as VOC-limited or transitional regimes where the four indicators largely showed differences. The O_3 formations in these areas were primarily VOC-limited according to $P_{H_2O_2}/P_{HNO_3}$ and showed a transition from VOC-limited to NO_x-limited at the surrounding grid cells. However, other indicators tended to assign the areas along and to the south of the river to transitional regimes. The fraction of the VOC-limited regimes in the area in Jiangsu with $P_{H_2O_2}/P_{HNO_3}$ ($\sim 13\,\%$) was considerably higher than that using $HCHO/NO_2$ and $HCHO/NO_y$ (4 %–5 %). NO_y, which is the least impacted by VOC emissions, attributed the fewest areas to the VOC-limited regimes ($\sim 2\,\%$) concerning O_3 formation. Accordingly, transitional regimes were the lowest using $P_{H_2O_2}/P_{HNO_3}$, $\sim 5\,\%$ compared to 13 %–15 % using $HCHO/NO_2$, $HCHO/NO_y$, and NO_y.

3.2 Evaluation of the photochemical indicators

Table 4 shows the accuracy of the photochemical indicators in splitting the O_3 formation regimes with thresholds derived in this study. As expected, the ErrB and OA for the application in Jiangsu in 2017 (see the case Sim_2017+Jiangsu in Table 4) were approximately 5 % and 95 %, respectively, as a result of the nature of the method (see Sect. 2.3). The values of ErrA were lower than ErrB, suggesting that chemical regimes determined by the indicator values were largely consistent with that based on O_3 changes when perturbing emissions. However, it is more likely that sensitivities indicated by O_3 changes do not necessarily correspond to indicator values in the correct intervals. Additionally, the ErrA_VOC and ErrA_NO_x for $P_{H_2O_2}/P_{HNO_3}$ were higher than that of the other indicators, likely due to less area associated with mixed O_3 sensitivity using $P_{H_2O_2}/P_{HNO_3}$ (see Table S2), which could increase the chance of misclassification.

The above evaluation also showed that emissions could have a minor effect on the performance of the indicators on a regional scale. The thresholds derived from the simulation in Jiangsu well identified O_3 sensitivities in other regions of the YRD (see the case Sim_2017+Other), where emissions were different (e.g., abundant biogenic VOCs in the southern YRD vs. dominance of anthropogenic emissions in Jiangsu) and with OAs greater than 98 % for all the indicators. This suggests that it is plausible to specify region-wide thresholds for photochemical indicators. In addition, the indicators can generally separate O_3 formation regimes in Jiangsu for the same period in 2018 (see the case Sim_2018+Jiangsu) when the meteorology could differ from that in 2017. However, $HCHO/NO_y$ and $HCHO/NO_2$ appeared to be more easily affected by meteorology, as indicated by the ErrB_NO_x that showed that many NO_x-limited grids had indicator values lower than the upper thresholds. The OAs were relatively high in the case when both the emissions and meteorology changed (see the case Sim_2018+Other), although the ErrB_VOC was remarkably higher. This was due to fewer VOC-limited grids in the YRD, half of which had indicator values within the transition intervals and thus were misclassified as the transitional regime. The evaluation showed that indicators could perform better in detecting O_3 formation regimes that were predominant. However, the drawback of the evaluation is that it does not account for grids that are neither VOC-limited nor NO_x-limited in terms of the O_3 formation based on the $\Delta O_{3\,NO_x}$ or the $\Delta O_{3\,VOC}$ (i.e., the white area in Jiangsu in Fig. 2d), and the uncertainties of the photochemical indicators in these areas are unknown.

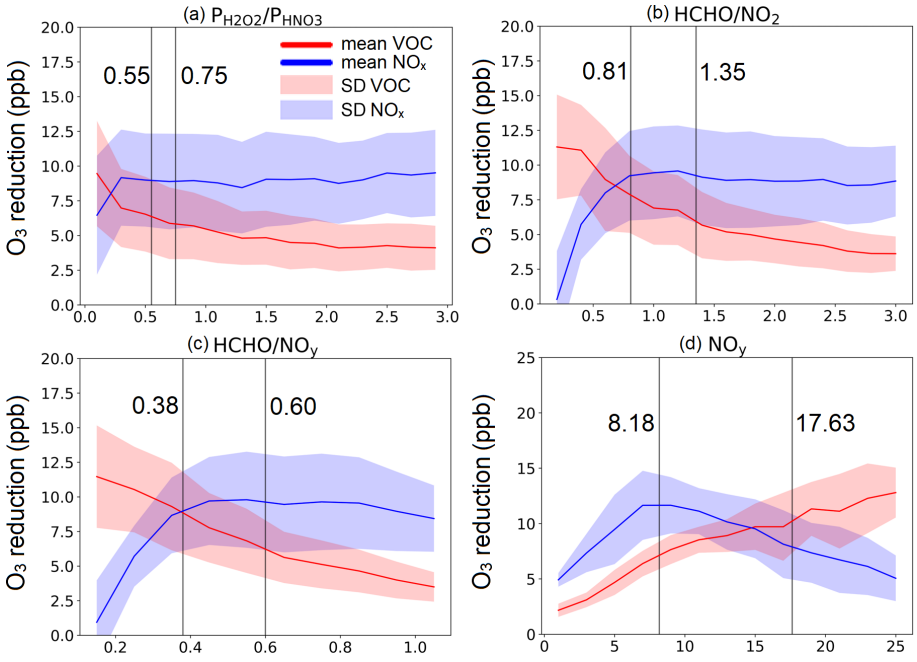

Figure 3. Relationships between the simulated O_3 reductions with the perturbed emissions and concurrent values of $P_{H_2O_2}/P_{HNO_3}$, $HCHO/NO_2$, $HCHO/NO_y$, and NO_y at all the grid cells in the domain. The red (blue) lines represent the average O_3 changes resulting from VOC (NO_x) emission reductions, with the shaded areas for the standard deviations. The thresholds derived in this study (see Table 3, with the method detailed in Sect. 2.3) are indicated by the gray vertical lines.

Table 3. Thresholds of the indicators derived in this study and reported in previous work.

Indicators	This study	Other studies
$P_{H_2O_2}/P_{HNO_3}$	[0.55, 0.75]	US: 0.06 (Tonnesen and Dennis, 2000a) China: 0.2 (Liu et al., 2010a) North China Plain: [0.08, 0.] (Zhang et al., 2020) East China: [0.30, 1.10] (Du et al., 2022)
$HCHO/NO_2$ (surface)	[0.81, 1.35]	US: [0.8, 1.8] (Tonnesen and Dennis, 2000b) East Asia: [0.5, 0.8] (Jin et al., 2017) East China: [0.36, 0.45] (Du et al., 2022) Yangtze River Delta: [0.55, 1.0] (Liu et al., 2021)
$HCHO/NO_y$	[0.38, 0.60]	US: 0.28 (Sillman, 1995) California: [0.5, 0.9] (Lu and Chang, 1998) Pearl River Delta: 0.41 (Ye et al., 2016)
NO_y	[8.18, 17.63]	US: 20 (Sillman, 1995) California: 5 (Lu and Chang, 1998) Germany: 7.78 (Vogel et al., 1999) Mexico City: 8.75 (Torres-Jardon et al., 2009)

3.3 Consistency with the O_3 isopleths

O_3 formation regimes identified by the indicator values with varied combinations of VOC and NO_x emissions were plotted together with the O_3 isopleths to examine the indicators for implications in effective emission control strategies. Figures 5 and S3–S4 show the comparison at the CCM, ZHM, and LS sites, respectively. As no significant variations were found at the three sites, only the plot for CCM is shown in the main text. The $P_{H_2O_2}/P_{HNO_3}$ value with the base emission points to a VOC-limited regime at the CCM site, whereas the isopleths suggest that a reduction in the NO_x emissions should lead to reduced O_3. This also happens in some cases with lower VOC and NO_x emissions, indicating that $P_{H_2O_2}/P_{HNO_3}$ is likely to underestimate the positive

Table 4. Evaluation of the photochemical indicators in the YRD (unit of %).

Case	Indicator	ErrA_VOCs	ErrB_VOCs	ErrA_NO_x	ErrB_NO_x	OA
Sim_2017+Jiangsu	$P_{H_2O_2}/P_{HNO_3}$	3.9	6.6	0.1	5.1	94.8
	$HCHO/NO_2$	2.9	5.7	0.0	5.1	94.9
	$HCHO/NO_y$	0.0	6.6	0.0	4.7	95.2
	NO_y	0.0	5.7	0.0	4.9	95.1
Sim_2017+Other	$P_{H_2O_2}/P_{HNO_3}$	7.4	0.0	0.0	2.0	98.0
	$HCHO/NO_2$	2.2	0.0	0.0	1.7	98.3
	$HCHO/NO_y$	2.1	0.0	0.0	0.7	99.3
	NO_y	0.0	12.8	0.0	1.3	98.6
Sim_2018+Jiangsu	$P_{H_2O_2}/P_{HNO_3}$	2.4	0.0	0.0	4.3	96.9
	$HCHO/NO_2$	0.0	0.8	0.0	7.0	94.8
	$HCHO/NO_y$	0.0	0.8	0.0	10.1	92.2
	NO_y	0.0	8.3	0.3	0.3	97.4
Sim_2018+Other	$P_{H_2O_2}/P_{HNO_3}$	2.7	7.0	0.1	1.7	98.2
	$HCHO/NO_2$	6.2	14.3	0.1	1.6	98.0
	$HCHO/NO_y$	0.5	12.2	0.1	1.2	98.5
	NO_y	0.0	51.3	0.1	1.3	97.3

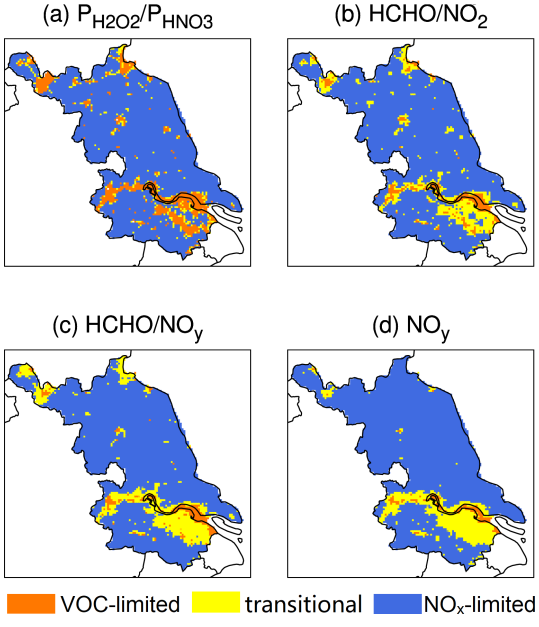

Figure 4. O_3 formation regimes based on the indicator values and thresholds in Table 3. The orange indicates a VOC-limited regime. The blue indicates a NO_x-limited regime. The yellow is associated with a transitional regime.

sensitivity of O_3 to NO_x. The indicators were assumed to have constant thresholds that do not change with emissions; this could partially explain the inconsistency of the indicators with the O_3 isopleths. The $P_{H_2O_2}/P_{HNO_3}$ values at the LS and ZHM sites showed similar results, except that the O_3 formation at the LS site shifted from VOC-limited to a transitional regime earlier with decreasing NO_x emissions than at the other two sites as indicated by the ratio.

It appears that $HCHO/NO_y$ was the most consistent with the O_3 isopleths among the four indicators, followed by $HCHO/NO_2$. Both $HCHO/NO_y$ and $HCHO/NO_2$ suggest that all three sites resided in transitional regimes under the base emission scenario, except for CCM using $HCHO/NO_2$, which showed that O_3 would respond to NO_x changes negatively. However, $HCHO/NO_y$ and $HCHO/NO_2$ had more emission scenarios assigned to transitional regimes compared with $P_{H_2O_2}/P_{HNO_3}$, which was in agreement with the spatial distributions shown in Fig. 4. This implies that the two indicators emphasize controlling both VOC and NO_x rather than a single pollutant. However, the HCHO levels could be affected by primary emissions (Liu et al., 2021) or be highly variable due to the dependence of isoprene on temperature (isoprene dominating HCHO production with intensive biogenic emissions) (Duncan et al., 2010). Therefore, the link between the $HCHO/NO_y$ (or $HCHO/NO_2$) values and the O_3–VOC–NO_x sensitivity and resulting emission control strategies of anthropogenic precursors (that are controllable) is more uncertain under certain conditions.

The O_3 formation at the CCM site was dominated by NO_x-limited regimes based on NO_y, which was predominantly affected by NO_x emissions, and did not show a sole sensitivity to VOCs (Fig. 5d). This was different from other indicators as well as the O_3 isopleths in terms of policy implications. The comparison between the O_3–VOC–NO_x sensitivity revealed by NO_y and the O_3 isopleths showed that the indicator tended to overestimate the response of O_3 to NO_x (i.e., the VOC-limited regimes were misclassified as transitional regimes in the upper left corner of Fig. 5d) or underestimate the O_3–VOC sensitivity (i.e., the transitional regimes were

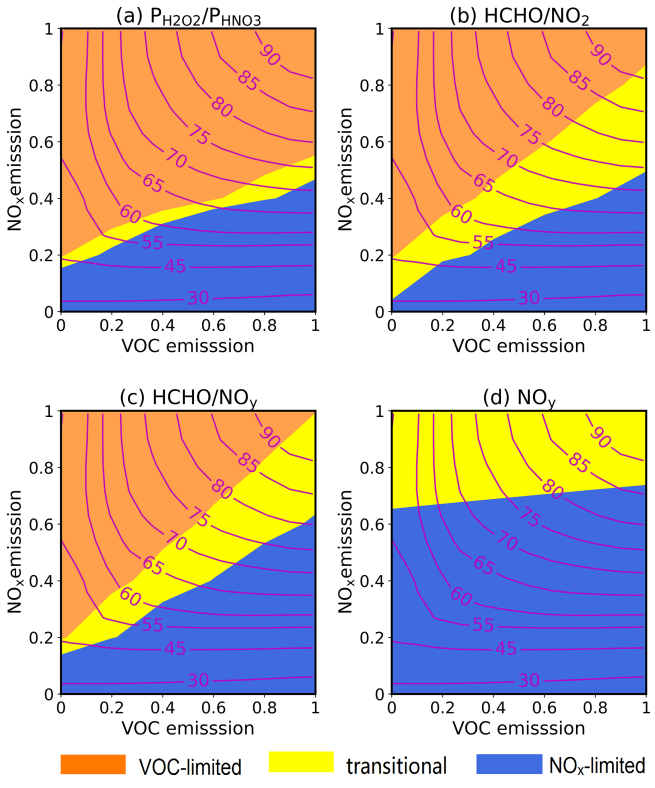

Figure 5. O_3 isopleths (red lines) overlap with the O_3 formation regimes (shading color) identified with $P_{H_2O_2}/P_{HNO_3}$, HCHO/NO_2, HCHO/NO_y, and NO_y (the thresholds given in Table 3) at the CCM site. The orange indicates a VOC-limited regime. The yellow indicates a transitional regime, and the blue indicates a NO_x-limited regime.

misclassified as NO_x-limited regimes in the middle left portion of Fig. 5d).

3.4 Uncertainties associated with the methodology

Apart from local emissions and meteorology that could partially explain the gap between the indicator thresholds proposed earlier and in this work, we found that the methodology to derive the thresholds could be slightly different and the impacts are unknown. Therefore, a series of tests were conducted to examine how those details in the methodology alter the thresholds of $P_{H_2O_2}/P_{HNO_3}$ (Fig. 6) and other indicators (Figs. S6–S8).

First, the VOC-limited (NO_x-limited) grid cells were defined as the locations where the reduction in O_3 as a response to the VOC (NO_x) reduction exceeded the O_3 reduction associated with the reduced NO_x (VOC) by more than 2, 3, and 6 ppb instead of the original 5 ppb (see Table 1). The threshold intervals are wider with higher criteria, e.g., the range of [0.3, 0.8] with sensitivity differences of >6 ppb versus [0.55, 0.75] with >5 ppb, leading to fewer VOC- or NO_x-limited grid cells based on the indicator and more transitional grid cells with less chance of misclassification (Fig. 6a). However, the sensitivity differences of 2–3 ppb are too small to differentiate sensitivity types of the grid cells using the indicators, as the 95th percentile of the indicator values at the VOC-limited grids is higher than the 5th percentile of the values at the NO_x-limited grids when determining the thresholds (see Sect. 2.3). Hence, the indicators are invalid. Similarly, if the relative changes in O_3 were applied to quantify the O_3–VOC–NO_x sensitivity, such as using the differences of 2 %, 5 %, or 8 % as the criteria, the derived thresholds would be considerably different as well (Fig. 6b). The relative changes make more sense since O_3 changes of ~ 5 ppb due to a certain amount of VOC or NO_x reduction are less likely to take place in locations with low O_3 than in relatively polluted regions. As a result, the grid cells with low O_3 are seemingly insensitive to precursors and were excluded from the VOC- or NO_x-limited grids that were used to derive the thresholds. This can particularly affect the lower limits of the thresholds with much fewer VOC-limited grids, as in this study, and vice versa.

In Fig. 6c, the VOC and NO_x emissions were individually reduced by 20 % or 40 % instead of 35 % but with a constant criterion of >5 ppb for the sensitivity differences. The lower reduction in emissions resulted in wider threshold intervals [0.18, 1.12] with a 20 % reduction versus [0.55, 0.75] with a 35 % reduction and [0.55, 0.60] with a 40 % reduction. This was similar to the case with higher criteria (Fig. 6a). In addition, if the VOC- or NO_x-limited grids were defined based on the S1 VOCs and S1 NO_x in the HDDM (see Table 1 and DDM1 in Fig. 6d), the indicator values for the VOC-limited grids and the NO_x-limited grids would overlap to a large extent, with the 95th percentile of the indicator values at the VOC-limited grids of 1.0, and the 5th percentile of the values at the NO_x-limited grids of 0.37. Therefore, the indicator could not be used. S1 VOCs and S1 NO_x approximate the O_3 changes with a 100 % reduction in the VOC and NO_x emissions, respectively, without considering the nonlinearity (i.e., higher-order sensitivities) in O_3 chemistry. This finding is consistent with Fig. 6c, which shows a quite narrow range of threshold intervals with more reduction in the precursor emissions. Additionally, the upper and lower thresholds derived with the DDM2 approach were 0.50 and 0.11, lower than 0.75 and 0.55, respectively. This was due to the lower O_3 changes estimated with the second-order Taylor expansions than with the perturbed simulations (Fig. S5), similar to the case with a 20 % reduction in the VOC or NO_x emissions and possibly reflecting the importance of higher-order terms in the HDDM as well. The results of HCHO/NO_2, HCHO/NO_y, and NO_y (Figs. S6–S8) were similar. They all indicated that the thresholds of the photochemical indicators are dependent on the methods or parameters in the methodology. This could be one of the major uncertainties in the application of indicators to determine O_3 chemical regimes.

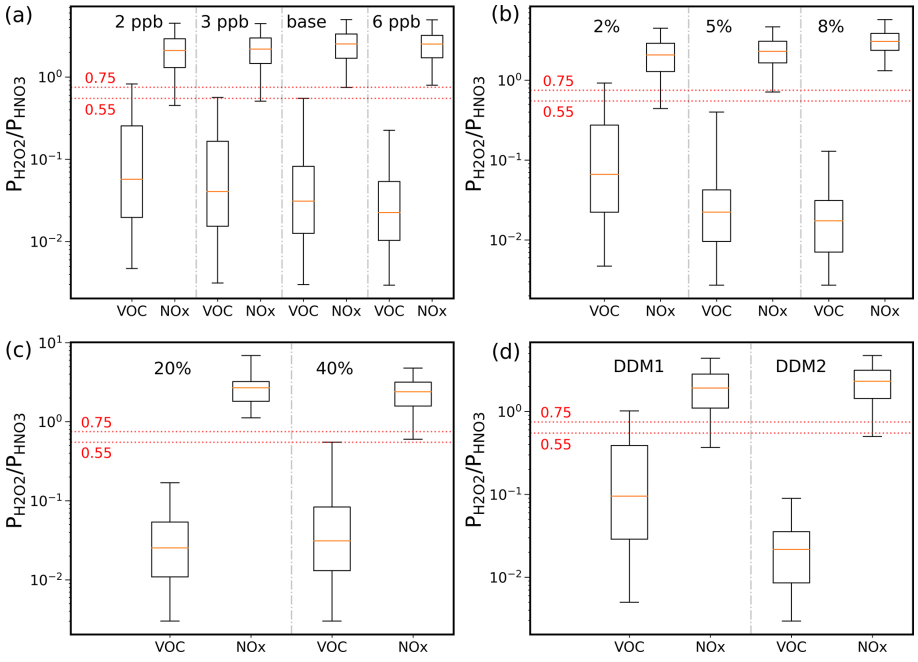

Figure 6. The percentile distributions of the $P_{H_2O_2}/P_{HNO_3}$ values at the VOC- or NO_x-limited grid cells with different setups in methodology. The boxes indicate the 25th and 75th percentiles of the indicator values with the median values marked with horizontal red lines in the boxes, and the whiskers extend to the 5th and 95th percentiles. In each group, the upper whisker of the box in the VOCs column and the lower whisker of the box in the NO_x column reflect the lower and upper values of the threshold intervals, respectively. The threshold intervals in Table 3 are indicated with dotted red lines.

4 Conclusions

This work revisited four photochemical indicators, including $P_{H_2O_2}/P_{HNO_3}$, $HCHO/NO_2$, $HCHO/NO_y$, and NO_y, in implications for O_3–NO_x–VOC sensitivity and emission control strategies using a case study in the YRD. The threshold intervals for Jiangsu (one of the provinces in the YRD) were derived, [0.55, 0.75] for $P_{H_2O_2}/P_{HNO_3}$, [0.81, 1.35] for the surface ratio of $HCHO/NO_2$, [0.38, 0.60] for $HCHO/NO_y$, and [8.2, 17.6] for NO_y, based on the relationship between the simulated indicator values and O_3 changes resulting from a 35 % reduction in the VOC or NO_x emissions. The indicators along with the localized thresholds were applied in other areas in the YRD, for a different simulation period, and with a combination of different locations and time to estimate the uncertainties related to the emissions and meteorology. The indicators displayed good performance in all cases, with OA values greater than 92 %, while $HCHO/NO_y$ and $HCHO/NO_2$ might have been susceptible to meteorological factors. However, $HCHO/NO_y$ and $HCHO/NO_2$ were the most consistent with the O_3 isopleths among the four indicators and could be informative for policymakers. The $P_{H_2O_2}/P_{HNO_3}$ ratio was less likely to attribute O_3 formation to mixed sensitivity and tended to underestimate the positive sensitivity of O_3 to NO_x compared to the isopleths. In contrast, NO_y, which was not constrained by the VOC abundance, overestimated the positive response of O_3 to NO_x and underestimated the O_3–VOC sensitivity in some conditions.

Importantly, the intrinsic characteristics of the indicators as well as the methods used to obtain the thresholds affected the effectiveness of the indicators. A series of sensitivity tests were conducted to investigate the impacts with respect to the criteria for the definition of VOC- or NO_x-limited grids; the number of VOC and NO_x emission perturbations; and the method, i.e., the HDDM tool versus emission reduction, to estimate the O_3–NO_x–VOC sensitivity in the first place. The results showed that the more stringent the criteria were (i.e., with larger the O_3 sensitivity differences or lower emission reductions using a given criterion), the wider the transition intervals were. This led to more attribution to the mixed O_3 sensitivity and showed a preference for concurrent control of both precursors. However, the indicator values at the VOC- and NO_x- limited grids could overlap in a large part and could not split the O_3 sensitivity when the criteria were set too low. Finally, the first-order coefficients in the HDDM alone with a specified sensitivity difference could not be used to derive thresholds of indicators in this study, while Taylor expansions with first- and second-order sensitivity coefficients could result in lower and broader threshold intervals.

Photochemical indicators have the advantage of identifying O_3 formation regimes promptly and are useful in policy implications. According to the case study in this work, we found that it was inappropriate to directly use the threshold

of 0.35 for $P_{H_2O_2}/P_{HNO_3}$ in the chemical transport models, as the value could be location-specific. More broadly, all of the indicators should be employed with specified thresholds that have been localized and thoroughly evaluated. In addition, the indicators could be different from each other. As such, it is necessary to understand the pros and cons of each indicator prior to their use.

Code and data availability. The CMAQ outputs are currently available upon request. All Python codes used to create any of the figures are available upon request.

Supplement. The supplement related to this article is available online at: https://doi.org/10.5194/acp-22-14799-2022-supplement.

Author contributions. XL, MQ, and JH conceived and designed the research. XL performed the simulations and analyzed the data. MQ, JH, HS, and JL contributed to result discussion. XL and MQ wrote the article with substantial contributions from all of the authors.

Competing interests. The contact author has declared that none of the authors has any competing interests.

Disclaimer. Publisher's note: Copernicus Publications remains neutral with regard to jurisdictional claims in published maps and institutional affiliations.

Acknowledgements. This work was supported by the Natural Science Foundation of Jiangsu Province (BK20200815) and the National Natural Science Foundation of China (42107117, 42007187, 42021004).

Financial support. This research has been supported by the Natural Science Foundation of Jiangsu Province (grant no. BK20200815) and the National Natural Science Foundation of China (grant nos. 42107117, 42007187, 42021004).

Review statement. This paper was edited by Zhibin Wang and reviewed by two anonymous referees.

References

An, J., Huang, Y., Huang, C., Wang, X., Yan, R., Wang, Q., Wang, H., Jing, S., Zhang, Y., Liu, Y., Chen, Y., Xu, C., Qiao, L., Zhou, M., Zhu, S., Hu, Q., Lu, J., and Chen, C.: Emission inventory of air pollutants and chemical speciation for specific anthropogenic sources based on local measurements in the Yangtze River Delta region, China, Atmos. Chem. Phys., 21, 2003–2025, https://doi.org/10.5194/acp-21-2003-2021, 2021.

Castell, N., Stein, A. F., Mantilla, E., Salvador, R., and Millán, M.: Evaluation of the use of photochemical indicators to assess ozone-NO_x-VOC sensitivity in the Southwestern Iberian Peninsula, J. Atmos. Chem., 63, 73–91, https://doi.org/10.1007/s10874-010-9158-x, 2009.

Chen, X., Jiang, Z., Shen, Y., Li, R., Fu, Y., Liu, J., Han, H., Liao, H., Cheng, X., and Jones, D. B.: Chinese regulations are working-why is surface ozone over industrialized areas still high? Applying lessons from northeast US air quality evolution, Geophys. Res. Lett., 48, e2021GL092816, https://doi.org/10.1029/2021GL092816, 2021.

Cohan, D. S., Hakami, A., Hu, Y., and Russell, A. G.: Nonlinear response of ozone to emissions: Source apportionment and sensitivity analysis, Environ. Sci. Technol., 39, 6739–6748, https://doi.org/10.1021/es048664m, 2005.

De Marco, A., Garcia-Gomez, H., Collalti, A., Khaniabadi, Y. O., Feng, Z., Proietti, C., Sicard, P., Vitale, M., Anav, A., and Paoletti, E.: Ozone modelling and mapping for risk assessment: An overview of different approaches for human and ecosystems health, Environ. Res., 211, 113048, https://doi.org/10.1016/j.envres.2022.113048, 2022.

Du, X., Tang, W., Cheng, M., Zhang, Z., Li, Y., Li, Y., and Meng, F.: Modeling of spatial and temporal variations of ozone-NO_x-VOC sensitivity based on photochemical indicators in China, J. Environ. Sci., 114, 454–464, https://doi.org/10.1016/j.jes.2021.12.026, 2022.

Duncan, B. N., Yoshida, Y., Olson, J. R., Sillman, S., Martin, R. V., Lamsal, L., Hu, Y., Pickering, K. E., Retscher, C., and Allen, D. J.: Application of OMI observations to a space-based indicator of NO_x and VOC controls on surface ozone formation, Atmos. Environ., 44, 2213–2223, https://doi.org/10.1016/j.atmosenv.2010.03.010, 2010.

Emery, C., Liu, Z., Russell, A. G., Odman, M. T., Yarwood, G., and Kumar, N.: Recommendations on statistics and benchmarks to assess photochemical model performance, J. Air Waste Manage., 67, 582–598, https://doi.org/10.1080/10962247.2016.1265027, 2017.

Feng, Z., Xu, Y., Kobayashi, K., Dai, L., Zhang, T., Agathokleous, E., Calatayud, V., Paoletti, E., Mukherjee, A., Agrawal, M., Park, R. J., Oak, Y. J., and Yue, X.: Ozone pollution threatens the production of major staple crops in East Asia, Nature Food, 3, 47–56, https://doi.org/10.1038/s43016-021-00422-6, 2022.

Gao, W., Tie, X., Xu, J., Huang, R., Mao, X., Zhou, G., and Chang, L.: Long-term trend of O_3 in a mega City (Shanghai), China: Characteristics, causes, and interactions with precursors, Sci. Total Environ., 603–604, 425–433, https://doi.org/10.1016/j.scitotenv.2017.06.099, 2017.

Gipson, G. L. and Young, J.: Process analysis, Science Algorithms of the EPA Models-3 Community Multiscale Air Quality (CMAQ) Modeling System, government document, US Environmental Protection Agency, Washington DC, 1999.

Hu, J., Chen, J., Ying, Q., and Zhang, H.: One-year simulation of ozone and particulate matter in China using WRF/CMAQ modeling system, Atmos. Chem. Phys., 16, 10333–10350, https://doi.org/10.5194/acp-16-10333-2016, 2016.

Jiménez, P. and Baldasano, J. M.: Ozone response to precursor controls in very complex terrains: Use of photochemical in-

dicators to assess O_3-NO_x-VOC sensitivity in the northeastern Iberian Peninsula, J. Geophys. Res.-Atmos., 109, D20309, https://doi.org/10.1029/2004JD004985, 2004.

Jin, X. and Holloway, T.: Spatial and temporal variability of ozone sensitivity over China observed from the Ozone Monitoring Instrument, J. Geophys. Res.-Atmos., 120, 7229–7246, https://doi.org/10.1002/2015JD023250, 2015.

Jin, X., Fiore, A. M., Murray, L. T., Valin, L. C., Lamsal, L. N., Duncan, B., Folkert Boersma, K., De Smedt, I., Abad, G. G., and Chance, K.: Evaluating a space-based indicator of surface ozone-NO_x-VOC sensitivity over midlatitude source regions and application to decadal trends, J. Geophys. Res.-Atmos., 122, 10439–10461, https://doi.org/10.1002/2017JD026720, 2017.

Kwok, R. H. F., Baker, K. R., Napelenok, S. L., and Tonnesen, G. S.: Photochemical grid model implementation and application of VOC, NO_x, and O_3 source apportionment, Geosci. Model Dev., 8, 99–114, https://doi.org/10.5194/gmd-8-99-2015, 2015.

Li, K., Jacob, D. J., Shen, L., Lu, X., De Smedt, I., and Liao, H.: Increases in surface ozone pollution in China from 2013 to 2019: anthropogenic and meteorological influences, Atmos. Chem. Phys., 20, 11423–11433, https://doi.org/10.5194/acp-20-11423-2020, 2020.

Li, L., Hu, J., Li, J., Gong, K., Wang, X., Ying, Q., Qin, M., Liao, H., Guo, S., Hu, M., and Zhang, Y.: Modelling air quality during the EXPLORE-YRD campaign – Part II. Regional source apportionment of ozone and $PM_{2.5}$, Atmos. Environ., 247, 118063, https://doi.org/10.1016/j.atmosenv.2020.118063, 2021.

Liang, J., Jackson, B., and Kaduwela, A.: Evaluation of the ability of indicator species ratios to determine the sensitivity of ozone to reductions in emissions of volatile organic compounds and oxides of nitrogen in northern California, Atmos. Environ., 40, 5156–5166, https://doi.org/10.1016/j.atmosenv.2006.03.060, 2006.

Liang, S., Li, X., Teng, Y., Fu, H., Chen, L., Mao, J., Zhang, H., Gao, S., Sun, Y., Ma, Z., and Azzi, M.: Estimation of health and economic benefits based on ozone exposure level with high spatial-temporal resolution by fusing satellite and station observations, Environ. Pollut., 255, 113267, https://doi.org/10.1016/j.envpol.2019.113267, 2019.

Liu, H., Wang, X. M., Pang, J. M., and He, K. B.: Feasibility and difficulties of China's new air quality standard compliance: PRD case of $PM_{2.5}$ and ozone from 2010 to 2025, Atmos. Chem. Phys., 13, 12013–12027, https://doi.org/10.5194/acp-13-12013-2013, 2013.

Liu, J., Li, X., Tan, Z., Wang, W., Yang, Y., Zhu, Y., Yang, S., Song, M., Chen, S., Wang, H., Lu, K., Zeng, L., and Zhang, Y.: Assessing the ratios of formaldehyde and glyoxal to NO_2 as Indicators of O_3–NO_x–VOC sensitivity, Environ. Sci. Technol., 55, 10935–10945, https://doi.org/10.1021/acs.est.0c07506, 2021.

Liu, X., Zhang, Y., Xing, J., Zhang, Q., Wang, K., Streets, D. G., Jang, C., Wang, W., and Hao, J.: Understanding of regional air pollution over China using CMAQ, part II. Process analysis and sensitivity of ozone and particulate matter to precursor emissions, Atmos. Environ., 44, 3719–3727, https://doi.org/10.1016/j.atmosenv.2010.03.036, 2010a.

Liu, X., Zhang, Y., Xing, J., Zhang, Q., Wang, K., Streets, D. G., Jang, C., Wang, W., and Hao, J.: Understanding of regional air pollution over China using CMAQ, part II. Process analysis and sensitivity of ozone and particulate matter to precursor emissions, Atmos. Environ., 44, 3719–3727, https://doi.org/10.1016/j.atmosenv.2010.03.036, 2010b.

Lu, C. H. and Chang, J. S.: On the indicator-based approach to assess ozone sensitivities and emissions features, J. Geophys. Res.-Atmos., 103, 3453–3462, https://doi.org/10.1029/97JD03128, 1998.

Lu, X., Hong, J., Zhang, L., Cooper, O. R., Schultz, M. G., Xu, X., Wang, T., Gao, M., Zhao, Y., and Zhang, Y.: Severe surface ozone pollution in China: A global perspective, Environ. Sci. Technol. Let., 5, 487–494, https://doi.org/10.1021/acs.estlett.8b00366, 2018.

Lu, X., Zhang, L., Wang, X., Gao, M., Li, K., Zhang, Y., Yue, X., and Zhang, Y.: Rapid increases in warm-season surface ozone and resulting health impact in China since 2013, Environ. Sci. Technol. Let., 7, 240–247, https://doi.org/10.1021/acs.estlett.0c00171, 2020.

Ma, M., Yao, G., Guo, J., and Bai, K.: Distinct spatiotemporal variation patterns of surface ozone in China due to diverse influential factors, J. Environ. Manage., 288, 112368, https://doi.org/10.1016/j.jenvman.2021.112368, 2021.

Martin, R. V., Fiore, A. M., and Van Donkelaar, A.: Space-based diagnosis of surface ozone sensitivity to anthropogenic emissions, Geophys. Res. Lett., 31, L06120, https://doi.org/10.1029/2004GL019416, 2004.

Murphy, J. G., Day, D. A., Cleary, P. A., Wooldridge, P. J., Millet, D. B., Goldstein, A. H., and Cohen, R. C.: The weekend effect within and downwind of Sacramento – Part 1: Observations of ozone, nitrogen oxides, and VOC reactivity, Atmos. Chem. Phys., 7, 5327–5339, https://doi.org/10.5194/acp-7-5327-2007, 2007.

Peng, Y.-P., Chen, K.-S., Wang, H.-K., Lai, C.-H., Lin, M.-H., and Lee, C.-H.: Applying model simulation and photochemical indicators to evaluate ozone sensitivity in southern Taiwan, J. Environ. Sci., 23, 790–797, https://doi.org/10.1016/s1001-0742(10)60479-2, 2011.

Qin, Y., Li, J., Gong, K., Wu, Z., Chen, M., Qin, M., Huang, L., and Hu, J.: Double high pollution events in the Yangtze River Delta from 2015 to 2019: Characteristics, trends, and meteorological situations, Sci. Total Environ., 792, 148349, https://doi.org/10.1016/j.scitotenv.2021.148349, 2021.

Shen, H., Sun, Z., Chen, Y., Russell, A. G., Hu, Y., Odman, M. T., Qian, Y., Archibald, A. T., and Tao, S.: Novel method for ozone isopleth construction and diagnosis for the ozone control strategy of Chinese cities, Environ. Sci. Technol., 55, 15625–15636, https://doi.org/10.1021/acs.est.1c01567, 2021.

Sheng, L., Qin, M., Li, L., Wang, C., Gong, K., Liu, T., Li, J., and Hu, J.: Impacts of emissions along the lower Yangtze River on air quality and public health in the Yangtze River delta, China, Atmos. Pollut. Res., 13, 101420, https://doi.org/10.1016/j.apr.2022.101420, 2022.

Sillman, S.: The use of NO_y, H_2O_2, and HNO_3 as indicators for ozone-NO_x-hydrocarbon sensitivity in urban locations, J. Geophys. Res., 100, 14175–14188, https://doi.org/10.1029/94JD02953, 1995.

Sillman, S.: The relation between ozone, NO_x and hydrocarbons in urban and polluted rural environments, Atmos. Environ., 33, 1821–1845, https://doi.org/10.1016/S1352-2310(98)00345-8, 1999.

Sillman, S.: Some theoretical results concerning O_3-NO_x-VOC chemistry and NO_x-VOC indicators, J. Geophys. Res., 107, 4659, https://doi.org/10.1029/2001jd001123, 2002.

Sillman, S., He, D., Pippin, M. R., Daum, P. H., Imre, D. G., Kleinman, L. I., Lee, J. H., and Weinstein-Lloyd, J.: Model correlations for ozone, reactive nitrogen, and peroxides for Nashville in comparison with measurements: Implications for O_3-NO_x-hydrocarbon chemistry, J. Geophys. Res.-Atmos., 103, 22629–22644, https://doi.org/10.1029/98JD00349, 1998.

Skeie, R. B., Myhre, G., Hodnebrog, Ø., Cameron-Smith, P. J., Deushi, M., Hegglin, M. I., Horowitz, L. W., Kramer, R. J., Michou, M., Mills, M. J., Olivié, D. J. L., Connor, F. M. O., Paynter, D., Samset, B. H., Sellar, A., Shindell, D., Takemura, T., Tilmes, S., and Wu, T.: Historical total ozone radiative forcing derived from CMIP6 simulations, npj Clim. Atmos. Sci., 3, 32, https://doi.org/10.1038/s41612-020-00131-0, 2020.

Sun, J., Qin, M., Xie, X., Fu, W., Qin, Y., Sheng, L., Li, L., Li, J., Sulaymon, I. D., Jiang, L., Huang, L., Yu, X., and Hu, J.: Seasonal modeling analysis of nitrate formation pathways in Yangtze River Delta region, China, Atmos. Chem. Phys., 22, 12629–12646, https://doi.org/10.5194/acp-22-12629-2022, 2022.

Tan, Z., Lu, K., Jiang, M., Su, R., Dong, H., Zeng, L., Xie, S., Tan, Q., and Zhang, Y.: Exploring ozone pollution in Chengdu, southwestern China: A case study from radical chemistry to O_3-VOC-NO_x sensitivity, Sci. Total Environ., 636, 775–786, https://doi.org/10.1016/j.scitotenv.2018.04.286, 2018.

Tang, G., Wang, Y., Li, X., Ji, D., Hsu, S., and Gao, X.: Spatial-temporal variations in surface ozone in Northern China as observed during 2009–2010 and possible implications for future air quality control strategies, Atmos. Chem. Phys., 12, 2757–2776, https://doi.org/10.5194/acp-12-2757-2012, 2012.

Tonnesen, G. S. and Dennis, R. L.: Analysis of radical propagation efficiency to assess ozone sensitivity to hydrocarbons and NO_x: 1. Local indicators of instantaneous odd oxygen production sensitivity, J. Geophys. Res.-Atmos., 105, 9213–9225, https://doi.org/10.1029/1999JD900371, 2000a.

Tonnesen, G. S. and Dennis, R. L.: Analysis of radical propagation efficiency to assess ozone sensitivity to hydrocarbons and NO_x: 2. Long-lived species as indicators of ozone concentration sensitivity, J. Geophys. Res.-Atmos., 105, 9227–9241, https://doi.org/10.1029/1999JD900372, 2000b.

Torres-Jardon, R., García-Reynoso, J. A., Jazcilevich, A., Ruiz-Suárez, L. G., and Keener, T. C.: Assessment of the ozone-nitrogen oxide-volatile organic compound sensitivity of Mexico City through an indicator-based approach: measurements and numerical simulations comparison, J. Air Waste Manage., 59, 1155–1172, https://doi.org/10.3155/1047-3289.59.10.1155, 2009.

Vogel, B., Riemer, N., Vogel, H., and Fiedler, F.: Findings on NO_y as an indicator for ozone sensitivity based on different numerical simulations, J. Geophys. Res.-Atmos., 104, 3605–3620, https://doi.org/10.1029/1998JD100075, 1999.

Wang, M., Chen, W., Zhang, L., Qin, W., Zhang, Y., Zhang, X., and Xie, X.: Ozone pollution characteristics and sensitivity analysis using an observation-based model in Nanjing, Yangtze River Delta Region of China, J. Environ. Sci., 93, 13–22, https://doi.org/10.1016/j.jes.2020.02.027, 2020.

Wang, N., Xu, J., Pei, C., Tang, R., Zhou, D., Chen, Y., Li, M., Deng, X., Deng, T., Huang, X., and Ding, A.: Air quality during COVID-19 lockdown in the Yangtze River Delta and the Pearl River Delta: Two different responsive mechanisms to emission reductions in China, Environ. Sci. Technol., 55, 5721–5730, https://doi.org/10.1021/acs.est.0c08383, 2021.

Wang, P., Guo, H., Hu, J., Kota, S. H., Ying, Q., and Zhang, H.: Responses of $PM_{2.5}$ and O_3 concentrations to changes of meteorology and emissions in China, Sci. Total Environ., 662, 297–306, https://doi.org/10.1016/j.scitotenv.2019.01.227, 2019.

Wang, X., Zhang, Y., Hu, Y., Zhou, W., Zeng, L., Hu, M., Cohan, D. S., and Russell, A. G.: Decoupled direct sensitivity analysis of regional ozone pollution over the Pearl River Delta during the PRIDE-PRD2004 campaign, Atmos. Environ., 45, 4941–4949, https://doi.org/10.1016/j.atmosenv.2011.06.006, 2011.

Wang, Y., Wild, O., Chen, X., Wu, Q., Gao, M., Chen, H., Qi, Y., and Wang, Z.: Health impacts of long-term ozone exposure in China over 2013–2017, Environ. Int., 144, 106030, https://doi.org/10.1016/j.envint.2020.106030, 2020.

Xie, M., Zhu, K., Wang, T., Yang, H., Zhuang, B., Li, S., Li, M., Zhu, X., and Ouyang, Y.: Application of photochemical indicators to evaluate ozone nonlinear chemistry and pollution control countermeasure in China, Atmos. Environ., 99, 466–473, https://doi.org/10.1016/j.atmosenv.2014.10.013, 2014.

Xu, J., Huang, X., Wang, N., Li, Y., and Ding, A.: Understanding ozone pollution in the Yangtze River Delta of eastern China from the perspective of diurnal cycles, Sci. Total Environ., 752, 141928, https://doi.org/10.1016/j.scitotenv.2020.141928, 2021.

Ye, C., Xue, C., Zhang, C., Ma, Z., Liu, P., Zhang, Y., Liu, C., Zhao, X., Zhang, W., and He, X.: Atmospheric hydrogen peroxide (H_2O_2) at the foot and summit of Mt. Tai: variations, sources and sinks, and implications for ozone formation chemistry, J. Geophys. Res.-Atmos., 126, e2020JD033975, https://doi.org/10.1029/2020JD033975, 2021.

Ye, L., Wang, X., Fan, S., Chen, W., Chang, M., Zhou, S., Wu, Z., and Fan, Q.: Photochemical indicators of ozone sensitivity: application in the Pearl River Delta, China, Front. Env. Sci. Eng., 10, 1–14, https://doi.org/10.1007/s11783-016-0887-1, 2016.

Zhang, Y., Zhao, Y., Li, J., Wu, Q., Wang, H., Du, H., Yang, W., Wang, Z., and Zhu, L.: Modeling ozone source apportionment and performing sensitivity analysis in summer on the North China Plain, Atmosphere, 11, 992–1011, https://doi.org/10.3390/atmos11090992, 2020.